frontiers in Materials

TYPE Original Research
PUBLISHED 30 September 2026
DOI 10.3389/fmats.2026.1970660

Check for updates

OPEN ACCESS

EDITED BY
Sanjay M R,
King Mongkut's University of Technology North Bangkok, Thailand

REVIEWED BY
Balaji Devarajan,
KPR Institute of Engineering and Technology, India
Joshuva Arockia Dhanraj,
Dayananda Sagar University, India

*CORRESPONDENCE
J.M.L. Reis,
jreis@id.uff.br

RECEIVED 17 August 2026
REVISED 25 August 2026
ACCEPTED 09 September 2026
PUBLISHED 30 September 2026

CITATION
Reis JML, Rohem HG, Bhering VPCC and Amorim FC (2026) Tensile properties of 3D-printed polylactic acid after extended UV radiation. *Front. Mater.* 13:1970660. doi: 10.3389/fmats.2026.1970660

COPYRIGHT
© 2026 Reis, Rohem, Bhering and Amorim. This is an open-access article distributed under the terms of the Creative Commons Attribution License (CC BY). The use, distribution or reproduction in other forums is permitted, provided the original author(s) and the copyright owner(s) are credited and that the original publication in this journal is cited, in accordance with accepted academic practice. No use, distribution or reproduction is permitted which does not comply with these terms.

Tensile properties of 3D-printed polylactic acid after extended UV radiation

J. M. L. Reis[1]*, H. G. Rohem[2], V. P. C. C. Bhering[1] and F. C. Amorim[3]

[1]Theoretical and Applied Mechanics Laboratory – LMTA, Mechanical Engineering Post-Graduate Program – PGMEC, Universidade Federal Fluminense UFF, Niteroi, Rio de Janeiro, Brazil, [2]Instituto Federal Fluminense – IFF, Campus Itaperuna, Itaperuna, Rio de Janeiro, Brazil, [3]Postgraduate Program in Mechanical Engineering and Materials Technology PPEMM, Celso Suckow da Fonseca Federal Center for Technology and Education CEFET/RJ, Rio de Janeiro, Brazil

Fused Deposition Modeling (FDM) of poly(lactic acid) (PLA) has expanded the use of bio-based thermoplastics in engineering applications; however, prolonged ultraviolet (UV) exposure can progressively affect their mechanical performance. This study investigates the tensile behavior of FDM-manufactured PLA specimens subjected to continuous UV-A radiation (61.4 W/m^2 at approximately 43 °C) for periods of up to 270 days. The experimental results revealed a progressive and non-uniform deterioration of the mechanical response with increasing exposure time. Ultimate tensile strength decreased from 53.46 $\pm$ 2.3 MPa for the reference condition to 35.51 $\pm$ 0.9 MPa after 270 days, corresponding to a reduction of approximately 33.6%, whereas the tensile modulus remained comparatively stable throughout the investigated exposure period. Elongation at break showed no consistent decreasing trend during the initial and intermediate exposure periods but decreased markedly after prolonged exposure, supporting the evolution toward a more brittle tensile response. Statistical analysis confirmed a significant effect of exposure time on tensile strength and elongation at break, while no significant effect was observed on tensile modulus. To complement the experimental investigation, a reduced-parameter phenomenological analytical formulation was employed to describe the evolution of the stress–strain response as a function of ultraviolet exposure time. The formulation satisfactorily reproduced the experimental stress–strain response within the investigated exposure and deformation ranges, providing a compact description of the time-dependent mechanical behavior of UV-aged FDM-manufactured PLA.

KEYWORDS
analytical modeling, fused deposition modeling (FDM), photo-oxidation, poly(lactic acid) (PLA), tensile strength, UV degradation

1 Introduction

As the demand for environmentally sustainable materials increases, poly(lactic acid) (PLA), a bio-based thermoplastic produced from renewable resources, has become one of the most widely used polymers in additive manufacturing (Mert et al., 2025; Ou-Yang et al., 2025). In addition to its renewable origin, PLA exhibits favorable mechanical properties and biocompatibility, supporting its use in applications ranging from packaging and biomedical products to engineering components (Portan et al., 2025).

Fused Deposition Modeling (FDM), also referred to as Fused Filament Fabrication (FFF), is one of the predominant additive manufacturing techniques for processing PLA. In this process, three-dimensional components are produced layer-by-layer through the controlled extrusion and deposition of molten thermoplastic filament (Gomes et al., 2025). FDM offers advantages such as relatively low cost, ease of processing, and the ability to manufacture complex geometries. However, the thermal history and layer-by-layer deposition inherent to the process can influence the crystallinity, molecular structure, interlayer bonding, and residual stresses of the printed material, thereby affecting its subsequent mechanical response and sensitivity to environmental exposure (Cuiffo et al., 2017).

The increasing use of PLA-based materials has also raised interest in their degradation and long-term stability under environmental conditions. Although PLA is generally regarded as a biodegradable polymer, its degradation behavior depends strongly on environmental conditions and exposure duration. Degradation can lead to the formation of oligomers, lactic acid, and other low-molecular-weight products, while changes in molecular structure may progressively affect the macroscopic properties of the material (Zimmermann et al., 2020).

Previous experimental studies have identified several physicochemical changes associated with UV degradation of PLA. Copinet et al. (2004), using FTIR spectroscopy and molecular-weight measurements, reported chemical changes accompanied by a reduction in molecular weight during PLA degradation under UV exposure. Gardette et al. (2011) investigated PLA under photo-oxidative conditions using infrared and UV-visible spectroscopy, DSC, and size-exclusion chromatography and reported oxidation of the polymer matrix together with the formation of photoproducts and changes in molecular weight. Quantitative molecular-weight analysis has also provided direct evidence of UV-induced chain scission in PLLA (Yasuda et al., 2011), while complementary FTIR, GPC, and H NMR analyses have further demonstrated chain scission and the formation of lower-molecular-weight species during PLA photodegradation (Olewnik-Kruszkowska et al., 2015). These experimental findings support photo-oxidation and chain scission as mechanisms associated with UV degradation of PLA. However, these mechanisms were not directly investigated in the present study and are therefore considered literature-supported interpretations of the observed mechanical deterioration.

Such molecular and microstructural modifications, as reported in the literature, can progressively influence the macroscopic mechanical behavior of PLA. Previous studies have reported surface deterioration, embrittlement, and reductions in tensile and impact properties following artificial or environmental aging of PLA-based materials (Spiridon et al., 2015; Hedayati et al., 2024). The extent of these changes depends on several factors, including the initial molecular structure, processing history, exposure conditions, and duration of aging. Furthermore, the formation of low-molecular-weight degradation products and carboxylic end groups may contribute to additional degradation reactions as exposure progresses (Jamshidi et al., 1988; Cam and Marucci, 1997).

Despite the growing literature on PLA degradation, the mechanical consequences of UV aging are commonly evaluated by comparing properties measured at discrete exposure periods. Such an approach is useful for quantifying changes in tensile strength, stiffness, or deformation capacity but does not, by itself, provide a continuous mathematical representation of how the complete stress–strain response evolves with exposure time. This limitation becomes particularly relevant when prolonged aging produces changes not only in the stress level sustained by the material but also in the shape of its tensile response.

Analytical and constitutive formulations provide a possible means of representing such evolution within a unified mathematical framework. Previous approaches, including the thermodynamically motivated formulations proposed by da Costa Mattos et al. (2009), da Costa Mattos et al. (2019), have demonstrated that complex nonlinear mechanical responses can be represented using a relatively small number of phenomenological parameters. The purpose of the present work is not to propose a new fundamental thermodynamic or continuum-damage theory, but rather to adapt this reduced-parameter analytical concept to describe the evolution of the tensile response of FDM-manufactured PLA as a function of prolonged UV exposure.

Accordingly, this study experimentally investigates the tensile behavior of 3D-printed PLA specimens subjected to continuous UV exposure for 15, 30, 60, 90, 120, 180, and 270 days. Particular attention is given to the evolution of the stress–strain response and ultimate tensile strength with exposure time. Statistical analysis is used to determine whether the observed reductions in tensile strength exceed the experimental variability.

To complement the experimental investigation, a phenomenological analytical formulation is employed in which the stress–strain response is governed by two exposure-dependent parameters with distinct mechanical roles. The parameter (a(t)) controls the stress scale of the response, whereas (b(t)) governs its curvature. After identification from the experimental curves, the evolution of these parameters is represented through continuous functions of UV exposure time. This procedure enables the tensile responses corresponding to different aging states to be described within a common analytical framework, rather than by independently fitting an unrelated constitutive equation to each exposure condition.

The principal contribution of the study therefore lies in combining an extended experimental investigation of FDM-manufactured PLA under prolonged UV exposure with a reduced-parameter, continuous exposure-time-dependent representation of its tensile response. Within the experimentally investigated domain, the formulation provides a compact means of describing the progressive changes in both stress level and stress–strain curvature associated with UV aging, while retaining a clear distinction between the phenomenological mechanical description and the underlying physicochemical degradation mechanisms.

2 Materials and methods

The raw material used in this study was a commercial white polylactic acid filament (trade name: PLA Plus) supplied by GTMax3D, Ltd. (Americana, Brazil). The filament had a nominal diameter of 1.75 ± 0.02 mm and a density of 1.24 g/cm^3. All specimens were fabricated using a commercial Fused Filament Fabrication (FFF) 3D printer (Core GT3, GTMax3D, Ltd., Brazil)

TABLE 1 Printing parameters for the test specimens.

3D printing parameter unit PLA plus	
Extrusion temperature ℃	220
Bed temperature ℃	60
Printing speed mm/s	80
Layer thickness mm	0.1
Raster width mm	0.4
Raster angle °	0
Infill density %	100

equipped with a 0.4 mm nozzle, operating at an extrusion temperature of 220 °C. The printing parameters are listed in Table 1.

Specimens were fabricated with an infill density of approximately 100% and a 0° raster orientation to ensure optimal mechanical performance along the primary loading axis, in accordance with ASTM D638 type 1 (Tymrak et al., 2014; ASTM, 2022).

The use of 100% infill density and a 0° raster orientation was intended to provide a controlled printing configuration in which the tensile response was predominantly governed by filaments aligned with the loading direction, while minimizing the influence of internal porosity and raster misalignment. These conditions should therefore not be interpreted as representative of all practical FDM configurations. Variations in raster orientation, infill density, layer thickness, and deposition strategy can modify interlayer bonding, void distribution, surface morphology, and load transfer mechanisms and may consequently affect both the initial tensile properties and their evolution during UV exposure. The influence of these manufacturing parameters on UV-induced mechanical degradation was outside the scope of the present study and should be addressed in future investigations.

For photo-oxidation testing, PLA specimens were mounted in a controlled UV exposure chamber equipped with six 15 W actinic fluorescent lamps with a nominal peak emission wavelength of 365 nm, within the UV-A spectral region. The maximum irradiance measured at the center of the chamber was approximately 61.4 W/m^2 (equivalent to 221 kJ/m^2·h). Based on this irradiance and continuous exposure, the estimated cumulative radiant exposure after the longest exposure period of 270 days was approximately 1.43 GJ/m^2. The chamber temperature was periodically monitored and remained approximately 43 °C during UV exposure. No separate thermal-aging control maintained at this temperature in the absence of UV radiation was included in the experimental program.

ASTM D904 (2021), Method A, Cycle II, was adopted as a procedural reference for defining the artificial-light exposure conditions, particularly continuous light exposure without added moisture. The standard was not used as a material-specific qualification procedure for PLA; rather, it provided a reproducible framework for controlled accelerated UV exposure. Therefore, the adopted exposure condition was intended to investigate prolonged UV-A aging under controlled dry conditions and not to reproduce the complete range of environmental factors associated with natural outdoor weathering.

Five specimens (n = 5) were retrieved at exposure intervals of 15, 30, 60, 90, 120, 180, and 270 days. Following each exposure period, the specimens were conditioned under the testing environment prior to tensile testing, while the reference specimens remained stored under laboratory conditions. Tensile properties were evaluated using a Shimadzu AG-X universal testing machine operating at a constant crosshead speed of 5 mm/min under controlled ambient conditions (23 °C and 50% relative humidity).

Engineering strain was determined using an extensometer attached directly to the specimens and maintained in place throughout the tensile test until specimen failure. Strain was calculated from the elongation measured by the extensometer relative to the initial gauge length. The tensile modulus was determined individually for each specimen in accordance with ASTM D638. The reported tensile modulus values correspond to the mean ± standard deviation of five specimens for each exposure condition. Elongation at break was determined from the engineering strain measured by the extensometer at specimen failure.

3 Results and discussion

3.1 Tensile tests

Hereafter, the uniaxial engineering stress, $\sigma(t)$, and engineering strain, $\varepsilon(t)$, are referred to simply as stress and strain, respectively, and are defined by Equations 1 and 2:

$$\sigma(t) = \frac{F(t)}{A_0} \tag{1}$$

$$\varepsilon(t) = \frac{\Delta L(t)}{L_0} \tag{2}$$

where L_0 is the gauge length of the specimen and A_0 is its initial cross-sectional area. At a given instant t, L_0 corresponds to the gauge section of the standard tensile specimen according to ASTM D638 (ASTM, 2022), while the applied axial force and the corresponding elongation are used to determine engineering stress and strain.

The tensile tests were conducted under controlled strain conditions. Figure 1 presents representative stress–strain curves for PLA specimens subjected to different periods of UV exposure.

The stress–strain curves reveal a progressive modification of the tensile response with increasing UV exposure time. For the reference condition and the shorter exposure periods, the curves exhibit broadly similar profiles. Their initial portions remain relatively close, suggesting that the initial response to tensile loading is comparatively preserved during the early stages of exposure. As deformation progresses, however, differences among the curves become more apparent, especially in the region approaching maximum stress and final failure.

The reference specimen exhibits a continuous increase in stress over a relatively broad strain range before reaching its maximum stress. A similar overall response is observed for the specimens subjected to the shorter exposure periods. Although some displacement among the curves is evident, their general shape and deformation range remain relatively comparable, indicating that the characteristic tensile response of the material is largely retained during the initial stages of UV exposure.

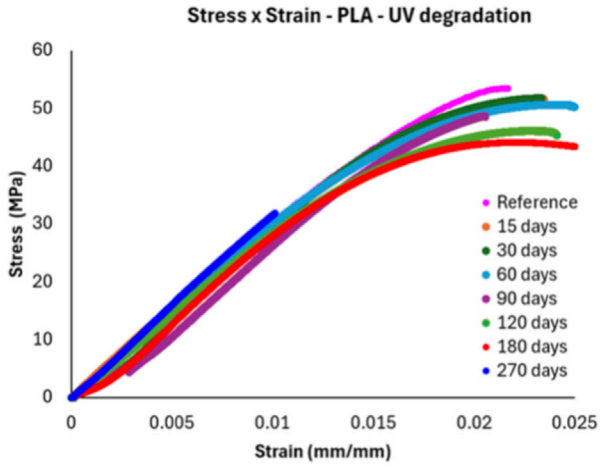

FIGURE 1
Typical experimental stress–strain curves of PLA subjected to different UV exposure periods.

As the exposure period increases, the curves progressively shift toward lower stress levels, particularly in the region preceding failure. This behavior becomes increasingly evident for the specimens subjected to longer UV exposure, suggesting a gradual deterioration in the load-bearing capability of the material. The most distinctive change is observed at prolonged exposure, where the stress–strain response terminates at a substantially lower strain than the curves corresponding to the reference and shorter exposure conditions. This pronounced reduction in deformation capacity suggests a transition toward a more brittle mechanical response after extended UV exposure.

Overall, the stress–strain curves indicate that the influence of UV radiation is comparatively moderate during the early stages of exposure but becomes progressively more evident with increasing exposure time. Furthermore, the changes are more pronounced near the maximum-stress and failure regions than in the initial portion of the curves, indicating that prolonged UV exposure particularly affects the ability of the material to sustain load and deformation prior to fracture.

The qualitative changes observed in the stress–strain response is corroborated by the ultimate tensile strength results presented in Table 2.

3.1.1 Statistical analysis

The effect of UV exposure time on ultimate tensile strength was evaluated using one-way analysis of variance (ANOVA). Prior to the analysis, the assumptions of normality and homogeneity of variance were examined. The Shapiro–Wilk test applied to the ANOVA residuals indicated no significant departure from normality ((W = 0.963), (p = 0.210)), while Levene's test showed no significant differences among the group variances ((F = 0.635), (p = 0.723)). Therefore, the assumptions required for parametric analysis were considered satisfied.

The one-way ANOVA revealed a highly significant effect of UV exposure time on ultimate tensile strength ((F(7,32) = 89.31), (p < 0.0001)). The magnitude of this effect was very large, with (η^2 = 0.951) and (ω^2 = 0.939), indicating that UV exposure condition accounted for a substantial proportion of the observed variability in tensile strength. The achieved statistical power of the omnibus ANOVA was greater than 0.999.

Tukey's Honestly Significant Difference (HSD) test was subsequently applied at the 95% confidence level to evaluate pairwise differences while controlling the family-wise Type I error rate. The resulting statistical groupings are presented in Table 2. Greater statistical overlap was observed among the shorter exposure periods. The reference and 15-day conditions were statistically similar, while the 30-day condition overlapped with both the reference/15-day group and the 60-day condition. In contrast, progressively greater differentiation emerged with increasing exposure duration, and the 270-day condition formed a distinct statistical group.

Together with the 95% confidence intervals of the group means, the large effect-size estimates demonstrate that the influence of prolonged UV exposure on tensile strength was not only statistically significant but also substantial relative to the experimental variability.

The effect of exposure time on tensile modulus and elongation at break was also evaluated using one-way ANOVA. For the tensile modulus, no statistically significant effect of exposure condition was observed ((F(7,32) = 1.60), (p = 0.171)). The modulus values remained within a relatively narrow range across the investigated conditions, indicating that the variations observed among the group means were not statistically distinguishable from the experimental variability at the 95% confidence level.

In contrast, exposure condition had a highly significant effect on elongation at break ((F(7,32) = 40.87), (p < 0.0001)). The magnitude of this effect was very large ((η^2 = 0.899), (ω^2 = 0.875)), indicating that exposure condition accounted for a substantial proportion of the observed variability in deformation at failure. Tukey's HSD *post hoc* test showed that the elongation at break after 270 days was significantly lower than that of all other exposure conditions. Although some differences were also observed among the intermediate exposure periods, the most pronounced change occurred after prolonged exposure, demonstrating a substantial reduction in deformation capacity at 270 days.

3.1.2 Effect of UV exposure on tensile strength

The results presented in Table 2 demonstrate a progressive deterioration in ultimate tensile strength with increasing UV exposure time. During the initial exposure period, the reduction was relatively limited. After 15 days, the ultimate tensile strength decreased by approximately 3.2% relative to the reference condition, while reductions of approximately 4.0% and 5.3% were observed after 30 and 60 days, respectively. These relatively modest changes indicate that the material retained most of its initial load-bearing capacity during the early stages of UV exposure.

A more pronounced deterioration developed as the exposure period increased. After 90 days, the reduction relative to the reference condition reached approximately 8.9%, increasing to approximately 13.8% after 120 days and 17.5% after 180 days. Therefore, the evolution of tensile strength suggests that the effect of UV exposure becomes progressively more important as irradiation continues.

TABLE 2 Ultimate tensile strength and tensile modulus of PLA as a function of UV exposure time.

Degradation period (days)	Ultimate tensile strength (MPa)*	Tensile modulus of elasticity (GPa)	Elongation at break (%)
Reference	53.46 ± 2.3^{a}	2.98 ± 0.21^{a}	2.19 ± 0.12 ^{ab}
15	51.74 ± 1.1 ^{ab}	2.92 ± 0.17^{a}	2.36 ± 0.19 ^{ab}
30	51.33 ± 1.5 ^{abc}	3.13 ± 0.26^{a}	2.33 ± 0.21 ^{ab}
60	50.64 ± 0.5 ^{bc}	3.04 ± 0.09^{a}	2.52 ± 0.22^{a}
90	48.69 ± 0.8 ^{cd}	3.18 ± 0.11^{a}	2.06 ± 0.16^{b}
120	46.08 ± 1.8 ^{de}	2.96 ± 0.13^{a}	2.42 ± 0.14^{a}
180	44.10 ± 1.2^{e}	3.15 ± 0.22^{a}	2.54 ± 0.18^{a}
270	35.51 ± 0.9^{f}	3.12 ± 0.12^{a}	1.02 ± 0.14^{c}

*Values are expressed as mean ± standard deviation (n = 5). Means sharing at least one superscript letter are not significantly different according to Tukey's HSD, test at the 95% confidence level.

The greatest deterioration was observed after 270 days, when the ultimate tensile strength was reduced by approximately 33.6% relative to the reference condition. Particularly noteworthy is the substantially greater decrease between 180 and 270 days compared with the changes observed during the earlier exposure intervals. This behavior indicates that the loss of mechanical performance does not evolve uniformly with exposure time. Instead, the experimental results suggest a comparatively gradual deterioration during the initial and intermediate stages, followed by a substantially stronger loss of tensile performance after prolonged exposure.

This trend is also evident when the retained tensile strength is considered. After 60 days of exposure, the material retained approximately 95% of its reference strength, and approximately 82% remained after 180 days. In contrast, after 270 days, only approximately 66% of the initial tensile strength was retained. The results therefore indicate that short-term UV exposure produces comparatively moderate changes in tensile performance, whereas prolonged exposure has a considerably more detrimental effect.

In contrast to the progressive reduction in ultimate tensile strength, the tensile modulus remained comparatively stable throughout the investigated exposure period, varying within a relatively narrow range of approximately 2.9–3.2 GPa (Table 2). No systematic decrease in stiffness with increasing exposure time was observed. This behavior indicates that the deterioration associated with prolonged exposure was more pronounced in the load-bearing capacity and deformation behavior of the material than in its initial tensile stiffness.

The elongation-at-break results provide further insight into the evolution of the deformation capacity of PLA. The reference specimens exhibited an elongation at break of 2.19% ± 0.12%, while values between 2.06% and 2.54% were observed for exposure periods up to 180 days, with no clear monotonic trend. After 270 days, however, elongation at break decreased markedly to 1.02% ± 0.14%, corresponding to a reduction of approximately 53% relative to the reference condition. This pronounced loss of deformation capacity, together with the reduction in tensile strength, supports the evolution toward a more brittle tensile response after prolonged exposure.

From an engineering perspective, the degradation can also be expressed through the residual-strength ratio, Equation 3,

$$\left(R_s(t) = \frac{\sigma_u(t)}{\sigma_{u,0}} \right) \tag{3}$$

Where $\sigma_u(t)$ is the UTS after exposure time (t) and $\sigma_{u,0}$ is the reference UTS.

Under the investigated UV exposure conditions, (R_s) decreased to approximately 0.66 after 270 days. A minimum acceptable value of (R_s) could therefore be defined according to the requirements and safety criteria of a particular application. However, conversion of this laboratory exposure time into an actual service-life prediction requires environmental correlation and application-specific design criteria and is beyond the scope of the present study.

The progressive reduction in tensile strength is consistent with mechanical degradation trends previously reported for PLA subjected to prolonged UV radiation. UV exposure may promote photo-oxidative processes capable of altering the polymer structure, including chain scission and the formation of oxidation products. However, the tensile tests performed in the present study do not directly identify the underlying chemical degradation mechanisms. Therefore, these processes should be regarded only as possible interpretations based on mechanisms previously reported in the literature, and their direct identification would require complementary physicochemical characterization.

Taken together, the stress–strain response and ultimate tensile strength results demonstrate a clear time-dependent modification of the mechanical behavior of PLA under UV exposure. While the material largely preserves its tensile response during the initial stages, prolonged irradiation results in progressive loss of load-bearing capacity and a marked reduction in deformation capability. The non-uniform evolution of these changes also suggests that exposure time should be explicitly incorporated when describing the mechanical behavior of UV-aged PLA. This time dependence provides the basis for the analytical formulation introduced in the following section, in which the evolution of the stress–strain response with UV exposure is represented through time-dependent material parameters.

It should be emphasized that the present results correspond to controlled UV-A aging under dry conditions. Because the

UV-exposed specimens were maintained at approximately 43 °C during irradiation, whereas the reference specimens were stored under laboratory conditions, the experimental design does not permit the effects of UV radiation to be completely separated from those associated with prolonged exposure to moderately elevated temperature. Accordingly, the observed mechanical changes should be interpreted as the response of PLA under the adopted UV-A exposure conditions, including the thermal environment within the exposure chamber, rather than as the isolated effect of UV radiation alone. A separate thermal-aging control maintained at the same temperature without UV irradiation would be required to quantify the individual contributions of thermal and photochemical aging.

Furthermore, the present exposure conditions should not be directly interpreted as representative of natural outdoor weathering. In service environments, UV radiation may act simultaneously with temperature variations, humidity, rainfall, and other environmental factors. In particular, moisture can promote hydrolytic degradation of PLA and may therefore modify the rate and extent of mechanical deterioration. Further studies incorporating thermal-aging controls, controlled humidity, wet–dry cycles, or natural weathering are required to establish the relationship between the present accelerated exposure conditions and long-term outdoor performance.

3.2 Mathematical model

The experimental results presented in the previous section demonstrate that UV exposure progressively modifies the tensile response of PLA and that these changes depend on the exposure period. To describe this time-dependent mechanical behavior through a reduced number of material parameters, an analytical formulation based on the phenomenological approach proposed by da Costa Mattos et al. (2009), da Costa Mattos et al. (2019) and subsequently applied by Reis et al. (2016) to account for the effects of aging and temperature on polymer tensile behavior was adopted. In these previous approaches, the parameters governing the stress–strain response were related to relevant environmental or material-state variables. Following this framework, the present study considers UV exposure time as the aging variable, and the stress–strain response at a given exposure time is expressed by Equation 4. The exponential form provides a reduced-parameter phenomenological representation of the nonlinear tensile response and is not intended as a unique thermodynamically derived constitutive law, but rather as a simple analytical formulation capable of describing the experimentally observed response with a limited number of parameters.

$$\sigma = a(t)[1 - \exp(-b(t)\varepsilon)] \tag{4}$$

where σ is the engineering stress, ε is the engineering strain, and t is the UV exposure time, expressed in days. The functions $a(t)$ and $b(t)$ are time-dependent parameters that describe the evolution of the tensile response as UV exposure progresses.

From Equation 4, parameter $a(t)$ defines the stress scale of the constitutive response. For increasing strain, the exponential term tends toward zero and the stress asymptotically approaches $a(t)$. Therefore, changes in $a(t)$ are directly associated with changes in the stress-carrying capacity represented by the model. A reduction in $a(t)$ with exposure time consequently reflects the progressive decrease in the stress level that the material can sustain.

Parameter $b(t)$, in turn, governs the curvature of the stress–strain response and determines how rapidly the stress approaches the asymptotic level defined by $a(t)$. The influence of both parameters on the initial response can be seen by differentiating Equation 5 with respect to strain, is presented in Equation 6:

$$\frac{d\sigma}{d\varepsilon} = a(t)b(t)[\exp(-b(t)\varepsilon)] \tag{5}$$

At the origin,

$$\frac{d\sigma}{d\varepsilon}\Big|_{\varepsilon=0} = a(t)b(t) \tag{6}$$

Thus, within the proposed formulation, parameter a represents the asymptotic stress level of the formulation and is associated with the maximum tensile strength of the material, whereas the product ab governs the initial tangent modulus predicted by the analytical formulation. Consequently, parameter b controls the curvature of the stress–strain response while being intrinsically coupled to both strength and stiffness. This relationship is particularly relevant to the interpretation of parameter identifiability, since variations in a may be accompanied by compensating variations in b while maintaining a similar initial modulus.

For each exposure condition, $a(t)$ and $b(t)$ were initially identified by fitting Equation 4 to the corresponding experimental stress–strain curve. Figure 2 presents the evolution of the identified parameters as a function of UV exposure time.

Figure 2 shows a systematic evolution of both parameters with UV exposure. Parameter $a(t)$ decreases as exposure time increases, which is consistent with the progressive downward shift of the stress–strain curves observed experimentally. Conversely, $b(t)$ increases with exposure time, indicating a progressive modification of the curvature of the tensile response.

The opposite trends exhibited by $a(t)$ and $b(t)$ are relevant to the representation of the degradation process. The decrease in $a(t)$ accounts primarily for the reduction in the stress scale, whereas the increase in $b(t)$ modifies the rate at which the stress approaches this level. Therefore, UV-induced changes in the mechanical response cannot be represented simply as a uniform reduction in strength; the shape of the stress–strain response also evolves with exposure time.

The uncertainty and practical identifiability of the model parameters were also evaluated from the nonlinear least-squares fits. A strong negative correlation was observed between a and b, which is consistent with the mathematical structure of the formulation. Since represents the maximum tensile strength and the initial tangent modulus is governed by ab, b is intrinsically coupled to both quantities and should not be interpreted as an independent material property. Thus, the observed correlation between a and b reflects, at least in part, the inherent coupling between strength, stiffness, and curvature in the proposed formulation. The confidence intervals of the fitted parameters were therefore considered when assessing the uncertainty of their identification.

The experimentally identified parameters were satisfactorily represented by power-law relationships within the investigated UV-exposure domain. Following the phenomenological modeling strategy adopted in previous studies, including Reis et al. (2016), the identified parameters were related to the relevant aging variable,

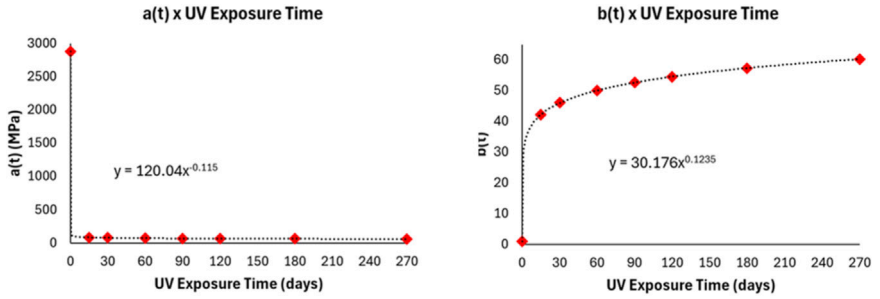

FIGURE 2
Evolution of the identified parameters as a function of UV exposure time.

TABLE 3 — Material constants.

Parameter	a_1 (MPa)	a_2	b_1	b_2
	120.04	−0.115	30.176	0.1235

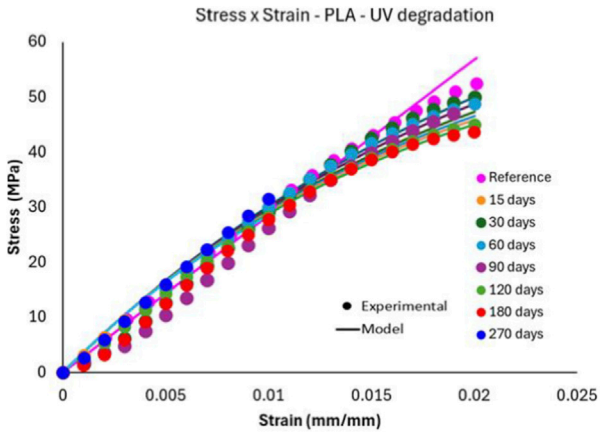

FIGURE 3
Comparison between experimental and calculated stress–strain curves of PLA at different UV exposure periods.

which in the present study is UV exposure time. The power-law relationships are defined for positive exposure times ($t > 0$), whereas the unexposed reference condition () is explicitly represented by the independently identified reference parameters a_{ref} and b_{ref}. Thus, the reference state is not obtained by extrapolating the power-law relationships to zero exposure time. Because these relationships were fitted to the same dataset used for parameter identification, they should be interpreted as descriptive correlations rather than as independently validated predictive laws. Accordingly, the time-dependent parameters are defined as Equation 7:

$$a(t) = \begin{cases} a_{ref}, t = 0 \\ a_1 t^{a_2}, t > 0 \end{cases} \quad (7)$$

$$b(t) = \begin{cases} b_{ref}, t = 0 \\ b_1 t^{b_2}, t > 0 \end{cases} \quad (8)$$

Where a_{ref} and b_{ref} are parameters identified for the unexposed reference condition a_1, a_2, b_1 and b_2 are material constants determined from the UV-exposed experimental data, and t is the UV exposure time in days. Because each time-dependent parameter is described by a two-constant power-law relationship, two exposure conditions are mathematically sufficient to determine the corresponding constants. Once and are determined for a given exposure time, the stress at a specified strain can be calculated directly from Equation 4. However, the predictive accuracy of a calibration based on only two exposure conditions has not been independently validated in the present study.

The identified values of the material constants are summarized in Table 3.

The signs of the identified exponents are consistent with the evolution observed in Figure 3. Since a_2 is negative, Equation 7 describes a progressive decrease in $a(t)$ with increasing exposure time. Conversely, the positive value of b_2 results in an increase in $b(t)$ according to Equation 8. The model therefore introduces the effect of UV exposure through two competing parameter evolutions: a decreasing stress-scale parameter and an increasing curvature parameter.

Substitution of Equations 7 and 8 into Equation 4 results in a single expression in which the tensile stress depends explicitly on both strain and UV exposure time, t, as Equation 9

$$\sigma = a_1 t^{a_2}\left[1 - \exp\left(-b_1 t^{b_2}\varepsilon\right)\right] \quad (9)$$

Equation 9 provides a continuous description of the evolution of the stress–strain response with UV exposure time, avoiding the need to define an independent set of constitutive parameters for each aging condition. In this sense, exposure time is introduced directly into the mechanical formulation as an internal degradation variable controlling the evolution of the tensile response.

It is important to emphasize that the proposed formulation is phenomenological. The parameters $a(t)$ and $b(t)$ are identified from the macroscopic stress–strain response and therefore characterize the mechanical consequences of UV exposure rather than specific molecular degradation mechanisms. Their evolution should consequently not be interpreted as direct evidence of particular physicochemical processes without complementary characterization.

TABLE 4 Goodness-of-fit metrics for the proposed analytical model at different UV exposure periods.

UV exposure	RMSE (MPa)	R^2
Reference	1.473	0.9912
15 days	0.659	0.9980
30 days	2.520	0.9756
60 days	1.511	0.9898
90 days	3.500	0.9490
120 days	1.246	0.9919
180 days	2.288	0.9743
270 days	1.993	0.9556

The proposed formulation is intended to describe the stress–strain behavior of the material as a function of UV exposure time within the experimentally investigated domain. Model identification and evaluation were restricted to the experimentally accessible tensile range, avoiding the region immediately preceding fracture. The model does not include a failure criterion and consequently does not predict the fracture strain. Extrapolation beyond the investigated exposure and deformation ranges should therefore be performed with caution.

The identified model parameters are specific to the commercial PLA grade and processing conditions investigated in this study and should not be regarded as universal constants for PLA. Although the mathematical framework may be applicable to other PLA grades or feedstocks, differences in material composition, molecular structure, crystallinity, additives, and processing conditions may modify the mechanical response and its evolution under UV exposure. Application of the formulation to other PLA materials therefore requires independent parameter identification and experimental verification.

The ability of the proposed formulation to reproduce the experimentally observed tensile behavior was evaluated by comparing the calculated stress–strain curves with the corresponding experimental results for the different UV exposure periods. These comparisons are presented in Figure 3.

Figure 3 compares the experimental stress–strain data with the responses obtained from the proposed analytical model for the different UV exposure periods. Overall, the model satisfactorily reproduces the main features of the tensile response and, more importantly, captures the systematic evolution of mechanical behavior with increasing UV exposure time.

The agreement between the experimental and calculated responses was also quantified using the coefficient of determination (R^2) and root-mean-square error (RMSE) over the modeled strain range ($\varepsilon \leq 2\%$), see Table 4. The R^2 values ranged from 0.949 to 0.998, while the RMSE values ranged from 0.659 to 3.500 MPa across the investigated exposure conditions, indicating satisfactory agreement between the experimental and calculated stress–strain responses.

For all exposure conditions, the model reproduces the nonlinear increase in stress with strain and the progressive separation of the stress–strain responses as deformation increases. The agreement between the experimental data and the analytical curves is particularly evident over the intermediate strain range, where the calculated responses closely follow the experimental points for most exposure conditions. This indicates that the two time-dependent parameters, $a(t)$ and $b(t)$, provide an adequate reduced-parameter representation of the evolution of the tensile behavior.

At low strain levels, some differences between the experimental points and analytical curves can be observed for certain exposure conditions. These deviations generally decrease as strain increases, and satisfactory agreement is maintained throughout the remaining strain range considered in the analysis. The deformation range considered in the analysis was selected to remain within the experimentally accessible response prior to fracture and was not limited because of deterioration in model agreement at increasing strain. Despite these local differences, the model successfully captures the relative evolution of the mechanical response associated with UV exposure. The progressive changes in the calculated curves are consistent with those observed experimentally, showing that the formulation is able to represent not only changes in the overall stress level but also modifications in the curvature of the stress–strain response. This behavior results from the combined evolution of $a(t)$ and $b(t)$, which respectively govern the stress scale and curvature of the analytical response.

An interesting feature of Figure 3 is that the differences among the exposure conditions become more evident as strain increases. At relatively low strains, the responses remain comparatively close, whereas a clearer separation develops at higher deformation levels. The model reproduces this general tendency, suggesting that the proposed formulation appropriately describes the increasing influence of UV exposure on the tensile response as deformation progresses.

Despite local differences between experimental and calculated responses, the formulation provides a satisfactory reduced-parameter representation of the UV-dependent tensile behavior within the investigated strain and exposure ranges. Because the model parameters were identified from the same experimental dataset used for comparison, these results demonstrate the descriptive capability of the formulation rather than constituting an independent validation of its predictive performance.

4 Conclusion

This study investigated the evolution of the tensile behavior of PLA subjected to prolonged UV exposure and proposed a time-dependent analytical formulation to describe the resulting changes in its mechanical response. Based on the experimental and modeling results, the following conclusions can be drawn:

- UV exposure progressively altered the tensile behavior of PLA. During the initial exposure periods, the stress–strain response remained relatively close to that of the reference material, whereas prolonged exposure produced increasingly evident changes in both load-bearing capacity and deformation behavior.
- Ultimate tensile strength decreased progressively with exposure time. The reduction remained relatively limited during the early stages of exposure but became more pronounced at longer periods. After 270 days, the material retained approximately

66% of its initial tensile strength, corresponding to an overall reduction of approximately 34%.

- In contrast to the progressive reduction in ultimate tensile strength, the tensile modulus remained comparatively stable throughout the investigated UV exposure period, with no systematic decreasing trend. This indicates that prolonged UV exposure had a more pronounced effect on the load-bearing capacity and deformation behavior of PLA than on its tensile stiffness.
- Elongation at break showed no consistent decreasing trend during the initial and intermediate exposure periods. However, a marked reduction was observed after prolonged exposure, indicating a substantial loss of deformation capacity and supporting the evolution toward a more brittle tensile response.
- Statistical analysis confirmed that UV exposure time had a significant effect on tensile strength. While partial statistical overlap was observed among the shorter exposure periods, a clear separation emerged at longer exposure times, demonstrating that the progressive loss of mechanical performance exceeded the experimental variability.

Overall, the results demonstrate that the mechanical degradation of PLA under UV exposure is strongly time-dependent and becomes particularly relevant after prolonged aging. The combination of experimental characterization and the proposed analytical formulation provides a useful framework for describing the evolution of the tensile response of UV-aged PLA. Nevertheless, the formulation should presently be regarded as a phenomenological description within the investigated exposure and strain ranges. Further studies involving independent experimental datasets, different PLA grades and printing conditions, longer exposure periods, and complementary physicochemical characterization would be valuable for assessing its broader applicability and predictive capability and for establishing relationships between the evolution of the model parameters and the underlying degradation mechanisms.

Data availability statement

The raw data supporting the conclusions of this article will be made available by the authors, without undue reservation.

Author contributions

JR: Conceptualization, Investigation, Methodology, Writing – original draft. HR: Conceptualization, Methodology, Writing – review and editing. VB: Data curation, Formal Analysis, Investigation, Writing – review and editing. FA: Investigation, Supervision, Visualization, Writing – review and editing.

Funding

The author(s) declared that financial support was not received for this work and/or its publication.

Acknowledgments

The authors acknowledge the Research Foundation of the State of Rio de Janeiro (FAPERJ), the Brazilian National Council for Scientific and Technological Development (CNPq) and Coordination for the Improvement of Higher Education Personnel (CAPES) for supporting part of the work presented here.

Conflict of interest

The author(s) declared that this work was conducted in the absence of any commercial or financial relationships that could be construed as a potential conflict of interest.

Generative AI statement

The author(s) declared that generative AI was not used in the creation of this manuscript.

Any alternative text (alt text) provided alongside figures in this article has been generated by Frontiers with the support of artificial intelligence and reasonable efforts have been made to ensure accuracy, including review by the authors wherever possible. If you identify any issues, please contact us.

Publisher's note

All claims expressed in this article are solely those of the authors and do not necessarily represent those of their affiliated organizations, or those of the publisher, the editors and the reviewers. Any product that may be evaluated in this article, or claim that may be made by its manufacturer, is not guaranteed or endorsed by the publisher.

References

ASTM D 904-99 (2021). *Standard Practice for Exposure of Adhesive Specimens to Artificial Light*.

ASTM D638-14 (2022). *Standard Test Method for Tensile Properties of Plastics*.

Cam, D., and Marucci, M. (1997). Influence of residual monomers and metals on poly (l-lactide) thermal stability. *Polym* 38, 1879–1884. doi: 10.1016/s0032-3861(96)00711-2

Copinet, A., Bertrand, C., Govindin, S., Coma, V., and Couturier, Y. (2004). Effects of ultraviolet light (315 nm), temperature and relative humidity on the degradation of polylactic acid plastic films. *Chemosphere* 55 (5), 763–773. doi: 10.1016/j.chemosphere.2003.11.038

Cuiffo, M. A., Snyder, J., Elliott, A. M., Romero, N., Kannan, S., and Halada, G. P. (2017). Impact of the fused deposition (FDM) printing process on polylactic acid (PLA) chemistry and structure. *Appl. Sci.* 7 (6), 579. doi: 10.3390/app7060579

da Costa Mattos, H. S., Minak, G., DiGioacchino, F., and Soldà, A. (2009). Modeling the superplastic behavior of Mg alloy sheets under tension using a continuum damage theory. *Mater Des.* 30, 1674–1679. doi: 10.1016/j.matdes.2008.07.013

da Costa Mattos, H. S., Brandão, J. F. S., Amorim, F. C., Araújo, P. V. S., and Reis, J. M. L. (2019). A unified expression to estimate the stress-strain curve of polyamides at different temperatures. *Mater. Res. Express* 6, 015304. doi: 10.1088/2053-1591/aae564

Gardette, M., Thérias, S., Gardette, J. L., Murillo, M. A., and Bussière, P. O. (2011). Photooxidation of polylactide (PLA). *Polym. Degrad. Stab.* 96 (4), 616–623. doi: 10.1016/j.polymdegradstab.2010.12.023

Gomes, D. A., Cusioli, L. F., Mantovani, D., Tusset, A. M., Parmegiani Marcucci, S. M., Lenzi, G. G., et al. (2025). Three-dimensional prototyping with PLA for the electrical sector: perspectives and challenges in material development. *Energies* 18 (11), 2844. doi: 10.3390/en18112844

Hedayati, R., Alavi, M., and Sadighi, M. (2024). Effect of degradation of polylactic acid (PLA) on dynamic mechanical response of 3D printed lattice structures. *Materials* 17, 3674. doi: 10.3390/ma17153674

Jamshidi, K., Hyon, S. H., and Ikada, Y. (1988). Thermal characterization of polylactides. *Polym* 29, 2229–2234. doi: 10.1016/0032-3861(88)90116-4

Mert, B. D., Nazligül, H., Aksaray, G., Mert, M. E., Seyedzavvar, M., and Kardaş, G. (2025). Sustainable energy solutions: 3D printed PLA-NiMo@Ag for green hydrogen production. *Int. J. Hydrogen Energy* 172, 151324. doi: 10.1016/j.ijhydene.2025.151324

Olewnik-Kruszkowska, E., Koter, I., Skopińska-Wiśniewska, J., and Richert, J. (2015). Degradation of polylactide composites under UV irradiation at 254 nm. *J. Photochem. Photobiol. A Chem.* 311, 144–153. doi: 10.1016/j.jphotochem.2015.06.029

Ou-Yang, H., Zhou, X., Zhang, Y., Wang, Y., Zhu, Z., Bai, J., et al. (2025). Interface enhancement of 3D printed CF/PLA composites by introducing "rigid-flexible" structures through multi-bond synergies. *Compos Struct.* 372, 119613. doi: 10.1016/j.compstruct.2025.119613

Portan, D. V., Koliadima, A., Kapolos, J., and Azamfirei, L. (2025). Biomimetic design and assessment via microenvironmental testing: from food packaging biomaterials to implantable medical devices. *Biomimetics* 10, 370. doi: 10.3390/biomimetics10060370

Reis, J. M. L., de Santanna, T., Coutinho, P. P., Monteiro, A. H., Teixeira, S. C. S., Chaves, E. G., et al. (2016). Coupled effect of ageing and temperature in the mechanical behaviour of a polyamide. *Polym. Test.* 53, 267–275. doi: 10.1016/j.polymertesting.2016.06.005

Spiridon, I., Darie-Nita, R. N., and Rusu, T. (2015). Behavior of PLA-based materials under artificial accelerated weathering. *J. Appl. Polym. Sci.* 132 (11), 41551–41560.

Tymrak, B. M., Kreiger, M., and Pearce, J. M. (2014). Mechanical properties of components fabricated with open-source 3-D printers under realistic environmental conditions. *Mater Des.* 58, 242–246. doi: 10.1016/j.matdes.2014.02.038

Yasuda, N., Tsukegi, T., Shirai, Y., and Nishida, H. (2011). Characteristic chain-end racemization behavior during photolysis of poly(l-lactic acid). *Biomacromolecules* 12 (9), 3299–3304. doi: 10.1021/bm200775r

Zimmermann, L., Dombrowski, A., Völker, C., and Wagner, M. (2020). Are bioplastics and plant-based materials safer than conventional plastics? *in vitro* toxicity and chemical composition. *Environ. Int.* 145, 106066. doi: 10.1016/j.envint.2020.106066